Mechanical Systems and Signal Processing 110 (2018) 333–348

Contents lists available at ScienceDirect

Mechanical Systems and Signal Processing

journal homepage: www.elsevier.com/locate/ymssp

Detection of half broken rotor bar fault in VFD driven induction motor drive using motor square current MUSIC analysis

Gurmeet Singh, V.N.A. Naikan *

Subir Chowdhury School of Quality and Reliability, IIT Kharagpur, 721302 West Bengal, India

ARTICLE INFO

Article history:
Received 22 May 2017
Received in revised form 6 January 2018
Accepted 2 March 2018
Available online 29 March 2018

Keywords:
Broken rotor bar
Induction motor
Fault diagnosis
MCSA
MUSIC
Motor square current signature analysis (MSCSA)

ABSTRACT

This paper presents a new method to diagnose half broken rotor bar (BRB) fault in induction motor drive, running under various load conditions using a variable frequency drive (VFD). VFDs are commonly used in industries to improve motor's efficiency, but at the same time it generates noise and this noise modulates with the line current. Noise leads to poor signal to noise ratio (SNR) as a result motor's fault diagnosis using current monitoring becomes a challenging task, especially when the fault is at incipient stage. One such case of half broken rotor bar (BRB), has been discussed in this paper. Conventional techniques like motor current signature analysis (MCSA) is found to be ineffective in detecting half BRB fault at normal load condition. In this paper authors have developed an algorithm that generates a pseudo-spectrum of square of the current signal, using multiple signal classification (MUSIC) techniques. The square of current signal generates more BRB fault frequency components and helps in easily diagnosing the fault. These fault frequency components are detected using the proposed algorithm. The work has been experimentally validated at various load conditions.

1. Introduction

Induction motors are commonly used as prime movers in most of the manufacturing and production industries due to its rugged design, low cost, easy control, high reliability and efficiency. However, its continuous operation under various electrical and mechanical stresses in adverse industrial and environmental conditions, leads to its deterioration which results in development of incipient faults. The incipient fault could result in failure of motor if it is not diagnosed at initial stage. Its sudden failure leads to increased downtime and production loss. Sometimes, the downtime cost may be much more than the actual cost of the motor. For example in an offshore plant the downtime losses due to motor failures can be as high as $25,000/h [1]. Condition monitoring of the motors helps in reducing motor downtime, by detecting fault at its initial level. This helps in taking corrective measures, planning maintenance schedule and inventory.

Distribution of failure of various motor components has been reported in percentage as: bearing (40%); stator (38%); rotor (10%) and others (12%), indicating that majority of failures are bearing and stator winding related [2,28]. Over the past two decades, condition monitoring and fault diagnosis of rotating machinery have been widely studied and reported [34–44]. Fault diagnosis techniques like Park's vector, extended Park's vector approach and thermographic analysis are found to be very effective in diagnosing winding faults while vibration monitoring helps in detecting bearing fault at initial stage

* Corresponding author.
E-mail addresses: singh@iitkgp.ac.in (G. Singh), naikan@hijli.iitkgp.ernet.in (V.N.A. Naikan).

https://doi.org/10.1016/j.ymssp.2018.03.001
0888-3270/

[3–8,27,43]. The commonly occurring faults i.e. bearing and stator winding can be detected using appropriate condition monitoring techniques at any load conditions [34,37]. Out the known types of failure, BRB is the third major cause of motor failure and is a serious concern. BRB if left undetected can cause multiple BRB faults or can also lead to insulation damage due to striking of the detached material from rotor bar with the stator, under the action of centrifugal force. Also, it can lead to eccentricity and thermal stress due to localized heating. Therefore, it is important to detect BRB fault at initial stage, so that necessary action could be taken on time.

Spectral estimation of motor current using extended Park's vector approach for diagnosing BRB fault has been proposed in [35,40]. The BRB diagnosis is based on the detection of DC component, $2sf$ and $4sf$ in the obtained spectrum. Extended Park's vector approach requires use of three current sensors, which increases its cost and data size. Also, this method cannot detect BRB fault at low load conditions. The other methods to detect BRB fault includes monitoring the fluctuations of motor current zero crossing instants [33], combination of stationary wavelet packet transform and multiclass wavelet support vector machines [30], supply voltage [11], magnetic flux [12–14], thermal field [15] and vibration signal [9,16]. The last two methods require site inspection or permanent installation of sensors on the motor, which is impractical in most of the industrial cases. Detecting fault using current monitoring is practically feasible and save time as it requires data collection from motor control panel only.

When a rotor bar is cracked, no current flows through that bar. As a result no magnetic flux is generated around the bar. It generates asymmetry in the rotor magnetic field by generating a non-zero backward rotating field which rotates at slip frequency with respect to the rotor [41]. It induces fault harmonic component in the stator current. These superimposed harmonics are used as BRB fault signature in MCSA. BRB fault frequencies are identified by the presence of fault frequencies component (1), as side bands near the supply frequency (f), where s = slip and k = 1, 2, 3 ... [2]. MCSA technique has been commonly used to detect the presence of BRB [9,10]. Multiple BRB faults are easily detected in MCSA, whereas initial level of BRB fault is difficult to detect, as modulation of supply current with BRB fault frequency is weak [17]. A continuous sample of long duration i.e. around 100 s is required to improve spectral resolution, which help in BRB fault detection [18]. However, under long duration of signal acquisition, load fluctuations are more likely to occur and can affect the results and decision making. While a short duration sample is less likely to suffer from load fluctuations, however it leads to poor resolution.

$$f_{brb} = (1 \pm 2ks) * f \tag{1}$$

Induction motors in industries are driven either through direct on line (DOL) or through variable frequency drives, VFD. A VFD is used for speed control applications like traction, compressors and mine mill drives. VFD is considered as energy saving drives but on the other hand it generates noise in the line currents. The noise generated by a VFD in the current signal reduces its signal to noise ratio (SNR). As a result it is difficult to detect the weak fault frequencies present in the MCSA spectrum [19].

In recent years a high resolution technique, Multiple Signal Classification (MUSIC) has been used to achieve satisfactory frequency resolution with samples of short duration. It has found to be very effective in detecting closely spaced sinusoids in a noisy signal [24]. MUSIC algorithm has been used to detect multiple BRB and single BRB faults [20,21,31]. Fault diagnosis at low load conditions have been analyzed using: Hilbert modulus with Fast Fourier Transform (FFT) [18], Hilbert modulus with Estimation of Signal Parameters via Rotational Invariance Technique (ESPRIT) [38] and Teager-Kaiser energy operator [39]. All these methods detect single and multiple BRB faults only.

Diagnosing half BRB using MCSA is not effective since fault signals are of weak amplitudes and they get embedded in the noise generated by VFD [22,23,29,32]. Limited literature had addressed the detection of half BRB fault, especially at light load conditions [29,36].

Literatures on BRB fault detection focuses on identifying sidebands of BRB fault frequency around supply frequency. This is the only feature that has been used to identify the presence of BRB fault. Spectrum of square of the motor's current known as motor square current signature analysis (MSCSA) generates additional BRB fault frequencies [25]. However, effectiveness of MSCSA technique in detecting half BRB fault by using a current signal corrupted by noise generated by VFD, has not been explored. Usage of more fault features will lead to easier fault diagnosis with lesser chances of false alarms.

A new approach has been proposed in this paper that uses Multiple Signal Classification (MUSIC) algorithm on the square of the current signal, in order to detect the half BRB fault at various load conditions. The proposed algorithm generates additional fault features which helps in clearly identifying the BRB fault. The authors tested this algorithm on simulated signals with additive white Gaussian noise and also experimentally validated on a VFD driven motor with seeded half BRB fault, running under various load conditions.

The rest of the paper is organized as follows; Section 2 deals with the introduction to MUSIC algorithm. Section 3 discusses the proposed algorithm namely Motor Square Current MUSIC (MSC-MUSIC) analysis. The effectiveness of MSC-MUSIC is verified through simulation in Section 4 and validated using an experimental setup in Section 5. Finally the conclusion drawn from this work is presented.

2. Music algorithm

A distorted or corrupted signal due to noise $x(t)$, sampled at a sampling interval t is given by (2).

$$x(t) = \sum_{j=1}^{p} A_j Cos(2\pi f_j + \Phi_j) + e(t) \quad (2)$$

where A_j, f_j and Φ_j are magnitude, frequency and phase of each sinusoid signal. The $e(t)$ indicates corrupted additive zero mean white noise and p indicates the total number of sinusoids of interest.

This techniques uses eigenvector decomposition of corrupted signal $x(t)$ into two orthogonal subspace i.e. actual signal and noise subspace (3). R_x is N X N autocorrelation matrix of $x(t)$, where N is the size of the estimated autocorrelation matrix and $N > p + 1$ [26]. R_s and R_n are autocorrelation matrixes of signal without noise and due to noise.

$$R_x = R_s + R_n \quad (3)$$

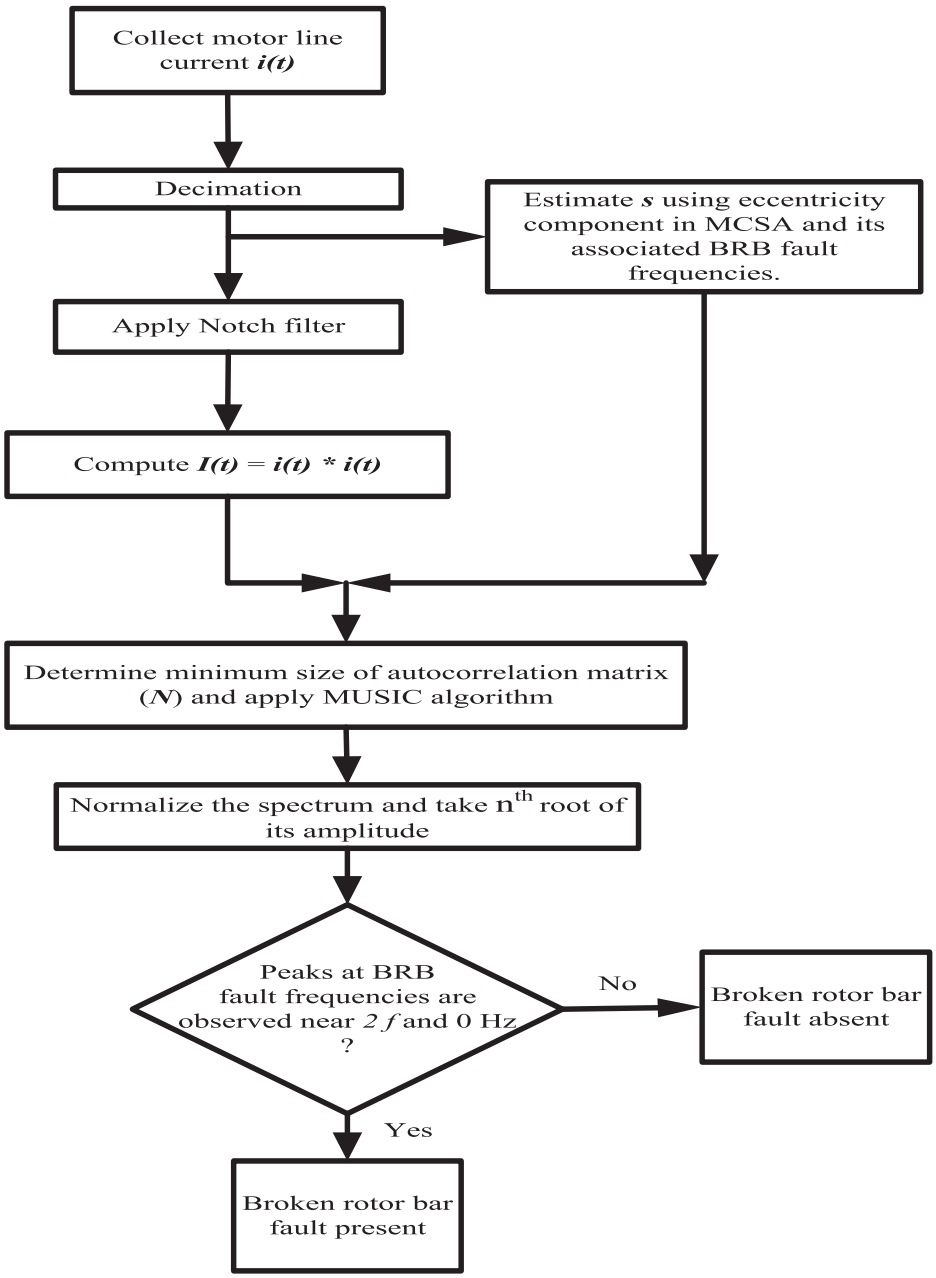

Fig. 1. Flowchart of the proposed MSC-MUSIC algorithm for detecting BRB fault.

The calculated eigenvalues of autocorrelation matrix are arranged in descending order. The first p eigenvalues corresponds to p sinusoids present in the signal and the rest $m = N - p$ corresponds to the noise present in the signal. Eigenvector e related to the first p eigenvalues belong to the R_s and eigenvector v related to rest of m eigenvalues belongs to R_n. The pseudo-spectrum peaks are found by (4) [26]. Though MUSIC has infinite theoretical resolution, in practice it has a finite limit because of perturbation of the signal autocorrelation matrix.

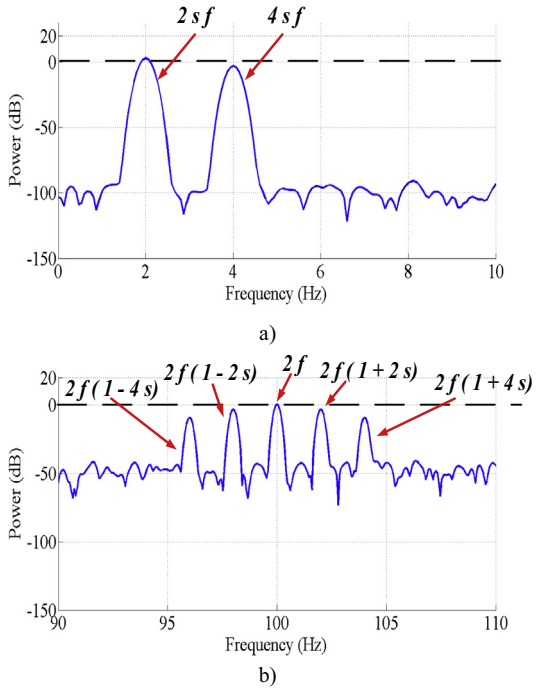

Fig. 2. Comparative analysis of generated I^2_{brb} component power at (a) 0 Hz and (b) 100 Hz with I_{brb} of 60 dB additive noise.

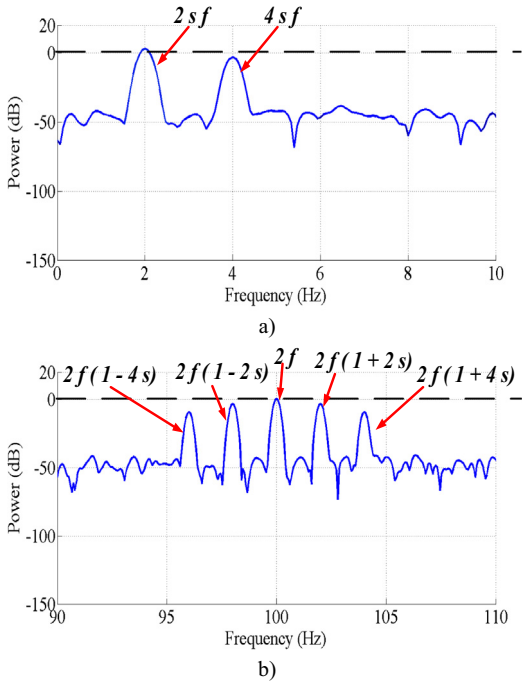

Fig. 3. Comparative analysis of generated I^2_{brb} component power at (a) 0 Hz and (b) 100 Hz with I_{brb} of 10 dB additive noise.

$$P_{MUSIC}(f) = \frac{1}{\sum_{i=p+1}^{M} |e(f)^H \cdot v_k|^2} \tag{4}$$

$$N = \frac{F_s}{sf} \tag{5}$$

Detection of closely spaced sinusoids in a noisy signal using MUSIC depends to a great extent on the sampling frequency F_s, slip s, supply frequency f and the size of the autocorrelation matrix N. Inappropriate selection of any of these may result in increased computational time and/or unresolved frequency components. The minimum size of the autocorrelation matrix has been calculated using (5) for each data window so that there is no overlapping of the fault frequency lobes with the fundamental [24]. Using this technique an algorithm has been proposed in the next section.

3. Proposed algorithm

Square of captured line current signal from the BRB faulty motor, provide new BRB fault frequency components: $2(1+s)f$, $2(1-s)f$, $2(1+2s)f$ and $2(1-2s)f$ are around $2f$ while $2sf$ and $4sf$ are around $0\,Hz$ [25]. Therefore, MSCSA highlights increased number of BRB fault frequency components compared to f_{brb} components in MCSA (1). Presence of a single side band in MCSA will generate 6 fault frequencies in MSCSA.

The generated additional fault frequencies are also embedded within the noise generated due to VFD. These frequencies are isolated from noise using MUSIC, which helps in identifying BRB fault easily and effectively. In this paper authors have developed an algorithm that uses MUSIC pseudo-spectrum on square of the obtained current signal, for detecting half BRB.

Table 1
Assumptions for simulated fault signals $I_{brb}(t)$.

SNR (dB)	F (Hz)	f-2sf (Hz)	f + 2sf (Hz)	a_1	a_2	a_3
10	50	49.8	50.2	0.9	0.009	0.0045
60	50	49.8	50.2	0.9	0.009	0.0045

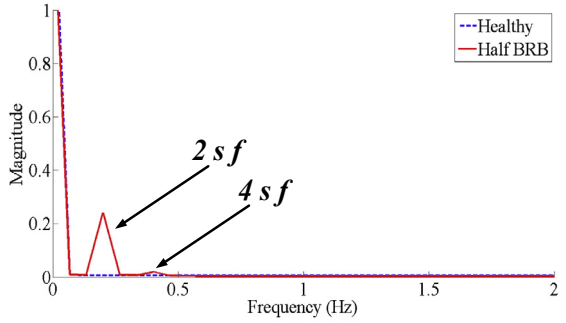

Fig. 4. MSC-MUSIC spectrum of signal with 60 dB added noise around (a) 0 Hz and (b) 100 Hz.

The developed algorithm uses motor's line current signal $i(t)$ for fault diagnosis, shown in Fig. 1. The captured current signal $i(t)$ is decimated (i.e. reduced the sampling frequency) to F_s. Decimation is a two step process in which signal is passed through a low pass filter in order to suppress aliasing to an acceptable level and later the filtered signal is downsampled to lower sampling frequency. Decimation improves frequency resolution for sample of fixed length which helps in detection of frequency components which are close to each other [23]. For a sample of fixed duration, decimation reduces the captured data size, which ultimately reduces its computation time.

Using MCSA, s is estimated through eccentric component f_e given in (6), where P = pole pair, n = 1, 3, 5, ... and m = 1, 2, 3, ... Later, the six new BRB fault frequencies are estimated using s and the minimum value of N are estimated, using (5).

$$f_e = nf \pm \frac{m(1-s)f}{P} \tag{6}$$

For MSC-MUSIC analysis, the decimated signal is passed through a notch filter. A notch filter will attenuate the fundamental component; as a result the fault frequency components close to the fundamental component are easily visible. The $I(t)$ is computed by taking square of $i(t)$ and later MUSIC algorithm is applied on the modified signal $I(t)$. Peaks at new BRB fault frequency components in the generated pseudo-spectrum, confirm the BRB fault.

The proposed algorithm generates additional BRB components which help in diagnosing half BRB effectively and confirms its presence even in light load conditions. The proposed algorithm has been validated through simulation as well as by experimental study. The results are discussed in the subsequent sections.

4. Simulated results

Simulated BRB fault signal $I_{brb}(t)$ is shown in (7). Where a_1, a_2 and a_3 represents the amplitudes of f, $(1-2s)f$ and $(1+2s)f$ and the signal (7) is corrupted by additive white gaussian noise n. For our analysis we have considered signal $I_{brb}(t)$ with additive white gaussian noise equal to 60 dB (high SNR) and 10 dB (low SNR) (7). Thereafter, square of $I_{brb}(t)$ is computed using (8). The comparative analysis of power of each BRB fault frequencies generated by $I^2_{brb}(t)$, using I_{brb} with 60 dB and 10 dB additive white noise, are shown in Figs. 2 and 3. The analysis is done by simulating the fault signal (7) with f = 50 Hz, f-$2sf$ = 48 Hz and $f + 2sf$ = 52 Hz with their amplitudes $a1 = a2 = a3 = 1$. Later $I^2_{brb}(t)$ has been computed (8) and it has been observed that the frequency component close to 0 Hz has higher power in comparison to the sidebands around $2f$.

$$I_{brb}(t) = a_1\cos(2\pi ft) + a_2\cos[2\pi(1-2s)ft] + a_3\cos[2\pi(1+2s)ft] + noise \tag{7}$$

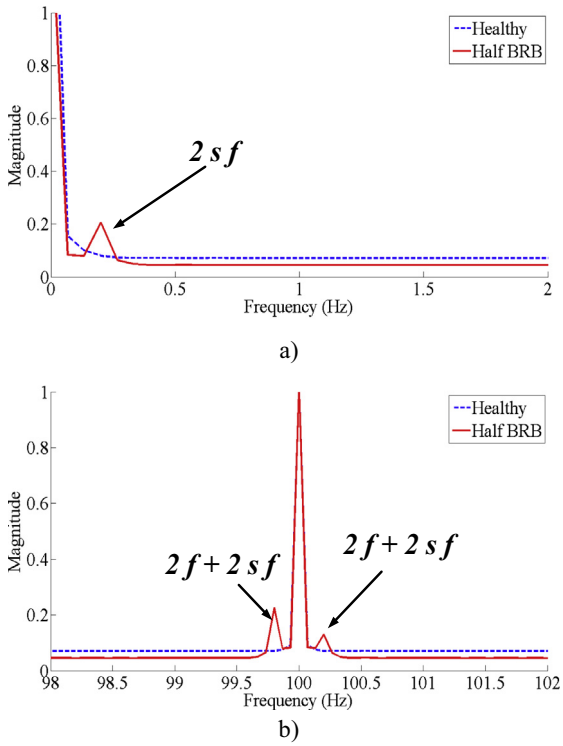

Fig. 5. MSC-MUSIC spectrum of signal with 10 dB added noise around (a) 0 Hz and (b) 100 Hz.

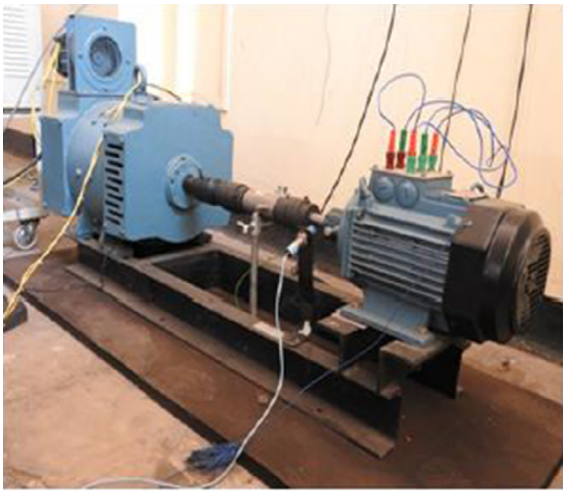

a)

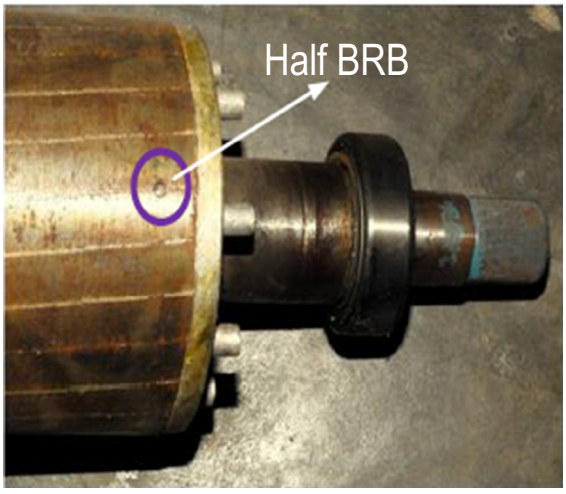

b)

Fig. 6. Images of the (a) experimental setup and (b) rotor with induced half BRB fault.

$$I_{brb}^2(t) = \left(\frac{a_1^2}{2}+\frac{a_2^2}{2}+\frac{a_3^2}{2}\right) + \left(\frac{a_1^2}{2}+a_2a_3\right)\cos(4\pi ft) + (a_1a_2+a_1a_3)\cos(4\pi sft) + a_2a_3\cos(8\pi sft) + a_1a_2\cos[4\pi(1-s)ft] + a_1a_3\cos[4\pi(1+s)ft] + \frac{a_2^2}{2}\cos[4\pi(1-2s)ft] + \frac{a_3^2}{2}\cos[4\pi(1+2s)ft] + noise^2 \quad (8)$$

To determine the effectiveness of the proposed algorithm in detecting weak BRB fault in a noisy signal. A low values of a_2 and a_3 with respect to a, has been considered with 60 dB and 10 dB of additive noise, shown in Table 1. The BRB fault current signals of t = 15 s duration with sampling rate 20 kS/s has been simulated. Later the signal is decimated to the desire sampling rate F_s equal to 500 S/s. The total length of sample L for the analysis is $F_s * t$ i.e. $500 * 15 = 7500$. The obtained spectral resolution is 1/15 Hz.

Table 2
Estimated BRB frequencies in MCSA.

BRB fault frequencies (Hz)						
BRB components	Load					
	5%	10%	20%	30%	50%	75%
2sf	0.3 Hz	0.8 Hz	1.3 Hz	1.9 Hz	2.4 Hz	4 Hz
f(1 − 2 s)	49.7 Hz	49.2 Hz	48.7 Hz	48.1 Hz	47.6 Hz	46 Hz
f(1 + 2 s)	50.3 Hz	50.8 Hz	51.3 Hz	51.9 Hz	52.4 Hz	54 Hz

The MUSIC algorithm is applied on the computed $I^2_{brb}(t)$ signal. The MUSIC algorithm requires the estimation of the value N and p. The value of N has been estimated using (5). Number of sinusoids of interest p can be estimated based on knowledge of fault pattern. For example, square of the three closely spaced sinusoids in $I_{brb}(t)$ (7) will generate $3 \times 3 = 9$ sinusoids in $I^2_{brb}(t)$. Out of them, 2 overlapping sinusoids and only 7 unique sinusoids are present (8). Therefore, p value higher than 9 can be considered to estimate the BRB fault frequency components in noisy signals. However, over estimation of p may lead to generation of random peaks in the spectrum. In order to detect simulated BRB faults effectively, p value equal to 10 has been considered for the proposed MSC-MUSIC algorithm.

Table 3
Estimated BRB frequencies in MSC-MUSIC and MSCSA analysis.

BRB fault frequencies (Hz)						
BRB components	Load					
	5%	10%	20%	30%	50%	75%
2sf	0.3 Hz	0.8 Hz	1.3 Hz	1.9 Hz	2.4 Hz	4 Hz
4sf	0.6 Hz	1.6 Hz	2.6 Hz	3.8 Hz	4.8 Hz	8 Hz
2f(1–2 s)	99.4 Hz	98.4 Hz	97.4 Hz	96.2 Hz	95.2 Hz	92 Hz
2f(1-s)	99.7 Hz	99.2 Hz	98.7 Hz	98.1 Hz	97.6 Hz	96 Hz
2f(1 + s)	100.3 Hz	100.8 Hz	101.3 Hz	101.9 Hz	102.4 Hz	104 Hz
2f(1 + 2 s)	100.6 Hz	101.6 Hz	102.6 Hz	103.8 Hz	104.8 Hz	108 Hz

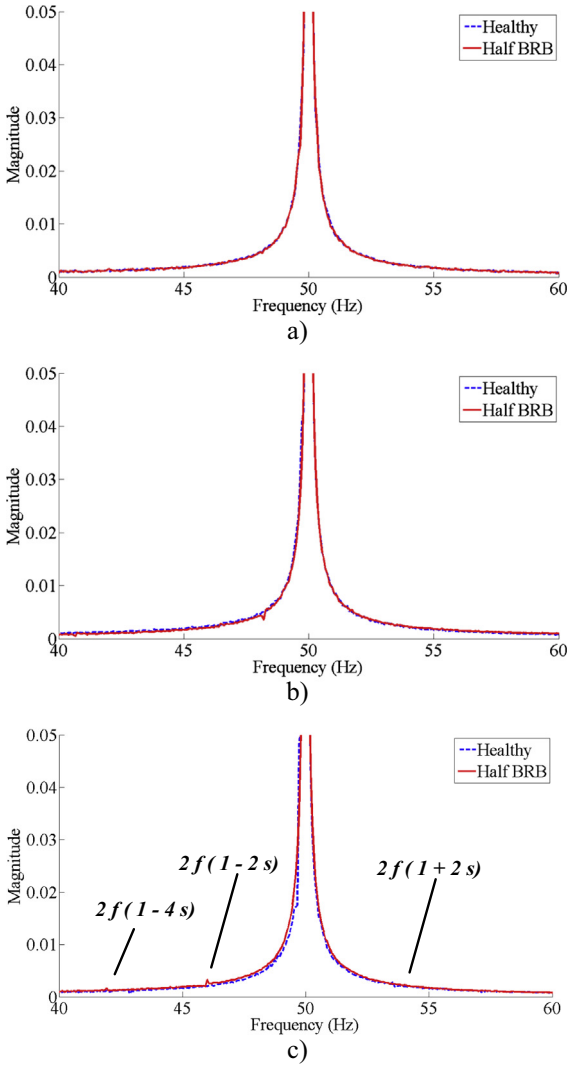

Fig. 7. MCSA spectrum of motor at (a) 5%, (b) 30% and (c) 75% load conditions.

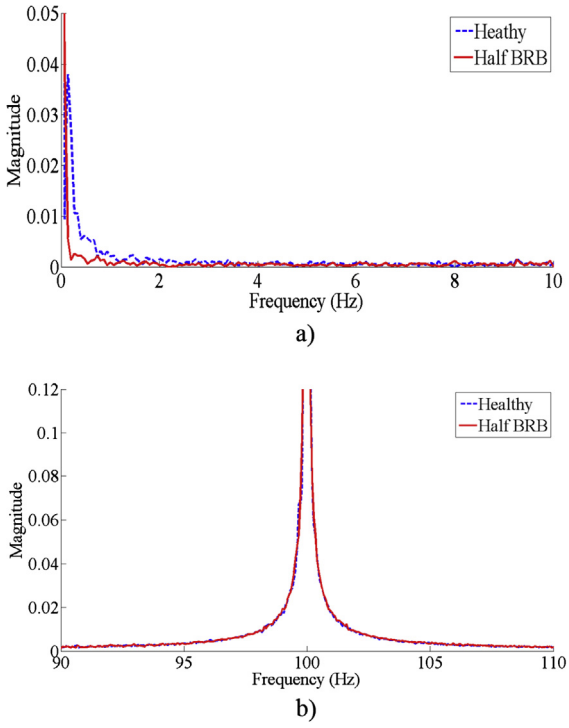

Fig. 8. MSCSA spectrum of motor running at 5% load condition near (a) 0 Hz and (b) 100 Hz.

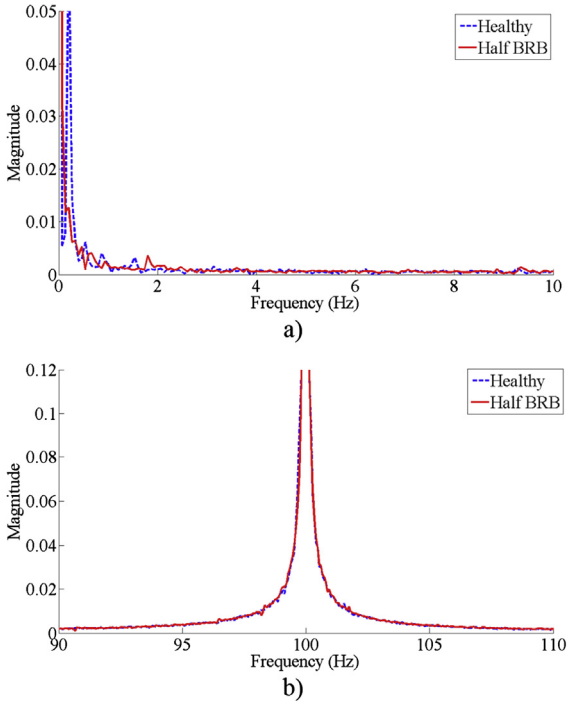

Fig. 9. MSCSA spectrum of motor running at 30% load condition near (a) 0 Hz and (b) 100 Hz.

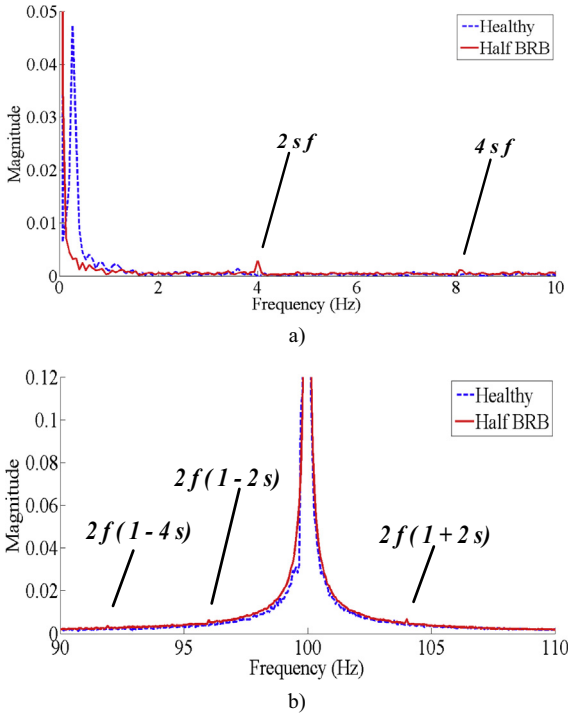

Fig. 10. MSCSA spectrum of motor running at 75% load condition near (a) 0 Hz and (b) 100 Hz.

Table 4
Analysis parameter for detecting BRB fault using MSC-MUSIC analysis.

Motor	Load	s	L = Fs * t	N (min)	M = N/(Fs * t)
Healthy	5	0.0028	7500	3572	0.48
	10	0.0052	7500	1924	0.26
	20	0.0108	7500	926	0.12
	30	0.016	7500	625	0.08
	50	0.0212	7500	472	0.06
	75	0.0348	7500	288	0.04
Half BRB	5	0.0028	7500	3572	0.48
	10	0.008	7500	1250	0.17
	20	0.0132	7500	758	0.1
	30	0.0188	7500	532	0.07
	50	0.024	7500	417	0.06
	75	0.04	7500	250	0.03

The MSC-MUSIC spectrum of the simulated current signal $I_{brb}(t)$ with additive white noise of 60 dB and 10 dB are shown in Figs. 4 and 5 respectively. Following observations have been made:

- The frequency components: *2f (1 ± 2 s)* and *4sf* as shown in (8), are not visible due to lower values of $a_2^2/2$, $a_3^2/2$ and a_2a_3 in signals with low SNR. However, signals with higher SNR value shows all the six fault frequency components presented in (8).
- Out of the six BRB fault frequency components, the *2sf* component is most dominating and easily visible due to its high power value.
- Presence of *2f (1 ± s)* and *2 s f* fault frequencies is enough to confirm the presence of BRB fault in the motor.

The proposed methodology is found to be effective in detecting BRB fault frequencies even in noisy signals. The proposed algorithm is also experimentally verified in the next section, by using a motor with induced half BRB fault.

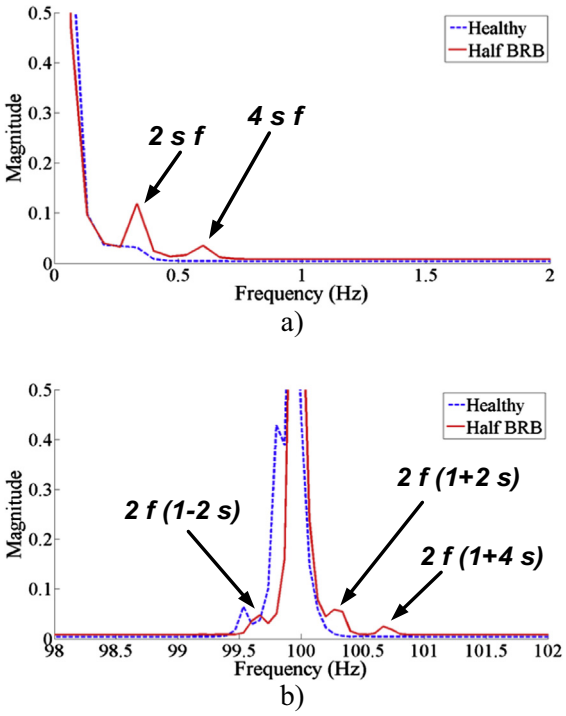

Fig. 11. MSC-MUSIC spectrum of motor running at 5% load condition near (a) 0 Hz and (b) 100 Hz.

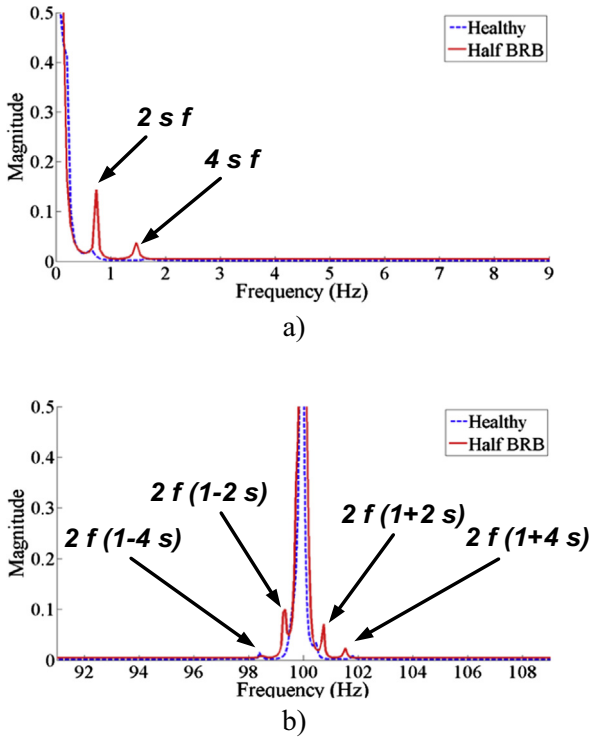

Fig. 12. MSC-MUSIC spectrum of motor running at 10% load condition near (a) 0 Hz and (b) 100 Hz.

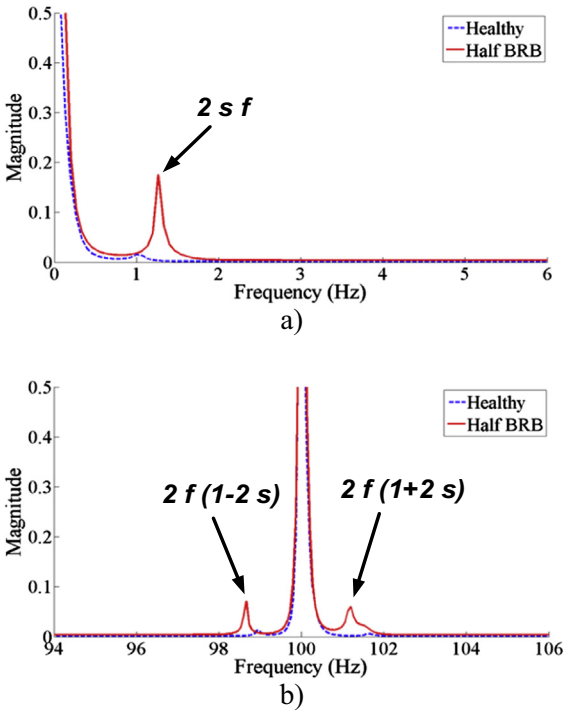

Fig. 13. MSC-MUSIC spectrum of motor running at 20% load condition near (a) 0 Hz and (b) 100 Hz.

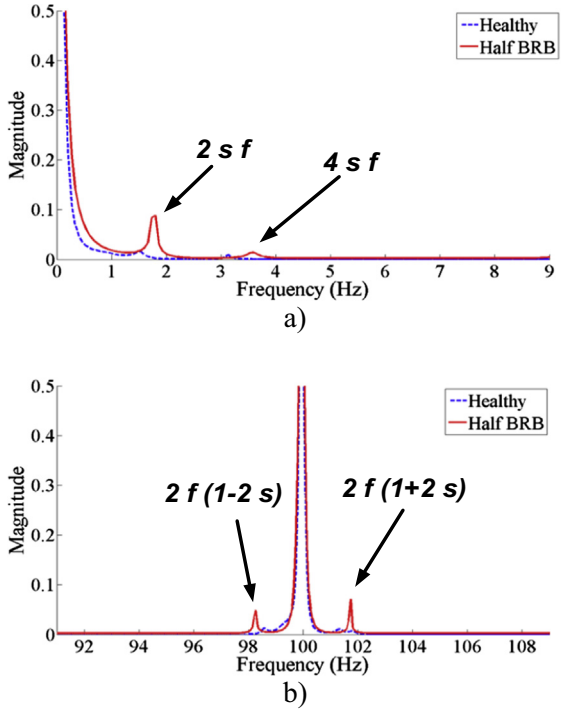

Fig. 14. MSC-MUSIC spectrum of motor running at 30% load condition near (a) 0 Hz and (b) 100 Hz.

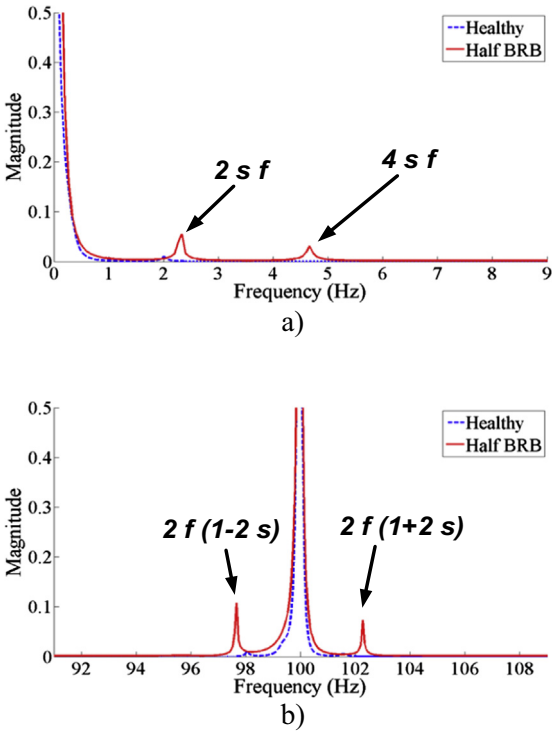

Fig. 15. MSC-MUSIC spectrum of motor running at 50% load condition near (a) 0 Hz and (b) 100 Hz.

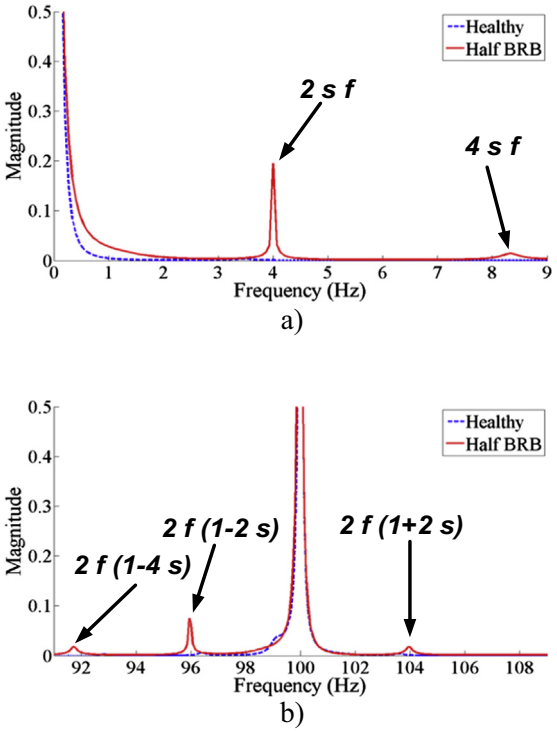

Fig. 16. MSC-MUSIC spectrum of motor running at 75% load condition near (a) 0 Hz and (b) 100 Hz.

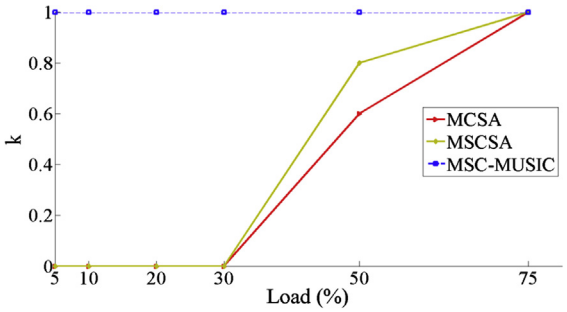

Fig. 17. Effectiveness of MSC-MUSIC analysis wrt MCSA and MSCSA technique in detecting half BRB fault at various load conditions.

5. Experimental setup and results

A 3 phase, 5 hp, 4 pole induction motor, with induced half BRB fault (drilled 9 mm of 20 mm of rotor bar width) is shown in Fig. 6. The faulty motor is driven by a VFD and a DC generator is coupled to the motor. The motor-generator set is loaded using resistive loads connected to the DC generator. Fluke i1000s clamp sensor and Yokogawa DL850E are used for acquisition of the current signal under various load conditions.

Signal of 15 s duration is collected at a sampling rate of 20 kS/s and it is decimated to desired sampling frequency F_s equal to 500 S/s. Decimation performs low pass filtering of the signal before down-sampling, reducing the aliasing effect. The data length L = Fs $*$ t = 7500 with frequency resolution of 1/15 Hz, is used for the analysis. The obtained MCSA and MSCSA spectrum is normalized by dividing the amplitude of each frequency component with the amplitude of *f* in case of MCSA and *2f* in MSCSA.

The estimated BRB fault frequencies under various load condition, used to diagnoses the BRB fault in MCSA and MSCSA/MSC-MUSIC, are shown in Tables 2 and 3. Detection of BRB fault frequencies using the conventional MCSA and MSCSA spectrum at 5%, 30% and 75% load conditions are shown in Figs. 7–10. It could be seen that both the methods are ineffective in detecting half BRB fault at 5% and 30% load conditions. Presence of fault is confirmed at 75% load condition, but the fault frequency components are weak. In practice, motor can operate at any load condition i.e. from light load to full load. Therefore, the algorithm should be effective in detecting the presence of fault under all load conditions. Therefore, this paper proposes MSC-MUSIC algorithm for the same.

The analysis parameters used for detecting BRB fault using MSC-MUSIC analysis are shown in Table 4. The current spectrum of 4 pole motor with BRB fault will have minimum 5 sinusoids i.e. 1 fundamental, 2 eccentric components and 1 BRB fault frequency sideband on either side of fundamental supply frequency *f*. Its square will generate 5 $\times$ 5 = 25 sinusoids. To effectively accommodate these components, the value of *p* equal to 30 has been considered in this work. The obtained results by using the proposed algorithm for diagnosing half BRB fault at 5%, 10%, 20%, 30%, 50% and 75% load conditions are shown in Figs. 11–16.

Square of the current drawn by the motor with BRB fault, will generates additional characteristic fault frequency components near *2f Hz* and *0 Hz*. However, in Fig. 11 b) peaks has also been observed near *2f* components of the MSC-MUSIC spectrum of healthy motor. These peaks could be due to load torque oscillation or noise generated by variable frequency drive. Therefore, in order to ensure BRB fault, the presence of at least *2f (1 ± s)* and *2sf* fault components is mandatory. Any deviation from these has been considered as negative BRB fault. This will help in clearly diagnosing BRB fault even at light loads conditions.

In order to test the robustness of the proposed method *wrt* MCSA and MSCSA, repeated experiments have been conducted and 10 samples under each load conditions of faulty motor have been collected. An indicator *k* has been used to test the robustness of the proposed method in detecting presence of half BRB fault at various load conditions (9). Clear peaks at *f (1 ± s)* in MCSA and peaks at *2f (1 ± s)* and *2sf* in MSCSA/MSC-MUSIC analysis has been considered as an indicator of BRB fault.

$$k = \frac{\text{number of times BRB fault diagnosed correctly under a given load condition}}{\text{number of faulty motor samples collected under given load condition}} \tag{9}$$

The effectiveness of the proposed MSC-MUSIC algorithm, with respect to MCSA and MSCSA is shown in Fig. 17. The MCSA and MSCSA have *k* value equal to zero up to 30% load condition. It indicates that these methods are not effective in detecting half BRB fault even at 30% load conditions. These techniques are effective in detecting fault only at high load conditions. For the proposed MSC-MUSIC algorithm, the *k* value is equal to one under all type of load conditions. This clearly shows the effectiveness of the proposed methodology in detecting half BRB fault, even at light load conditions.

6. Conclusion

VFD generates noise, which corrupts the motor current signal. As a result, the conventional MCSA technique is not effective in detecting half BRB fault, even when motor runs at normal load conditions. MCSA generates minimum two BRB fault

frequency components around *f* (supply frequency), while square of current signal generates additional BRB fault frequency components. These fault frequency components are near *0 Hz* and *2f Hz*. In MSCSA these fault frequency components are lost in the noise; as a result this technique is also not effective in diagnosing half BRB fault even at nominal load conditions. This paper has proposed an algorithm which performs MUSIC analysis on square of the motor current signal *viz.*, Motor Square Current MUSIC analysis (MSC-MUSIC). The algorithm can easily detect the additionally generated BRB fault components due to square of the line current, which the MSCSA fails to detect. It is capable of detecting half BRB fault even at light load condition. In this way the presented algorithm helps in confirming the presence of fault at incipient level. Therefore, it can help in planning maintenance activities in advance and minimizing the possibility of unexpected breakdown of the motor.

References

[1] S. Grubic, J.M. Aller, B. Lu, T.G. Habetler. A survey of testing and monitoring methods for stator insulation systems in induction machines, in: Presented at IEEE International Conference on Condition Monitoring and Diagnosis CMD, 2008.
[2] W.T. Thomson, M. Fenger, Current signature analysis to detect induction motor faults, IEEE Industry Appl. Mag. 7 (4) (2001) 26–34.
[3] A.M. Cardoso, S.M.A. Cruz, D.S.B. Fonseca, Inter-turn stator winding fault diagnosis in three-phase induction motors, by Park's vector approach, IEEE Trans. Energy Convers. 14 (3) (1999) 595–598.
[4] A. Gandhi, T. Corrigan, L. Parsa, Recent advances in modeling and online detection of stator interturn faults in electrical motors, IEEE Trans. Indust. Electron. 58 (5) (2011) 1564–1575.
[5] S.M. Cruz, A.M. Cardoso, Stator winding fault diagnosis in three-phase synchronous and asynchronous motors, by the extended Park's vector approach, IEEE Trans. Indust. Appl. 37 (5) (2001) 1227–1233.
[6] A. Bellini, F. Filippetti, C. Tassoni, G.A. Capolino, Advances in diagnostic techniques for induction machines, IEEE Trans. Indust. Electron. 12 (55) (2008) 4109–4126.
[7] G. Singh, T.C.A. Kumar, V.N.A. Naikan, Induction motor inter turn fault detection using infrared thermographic analysis, Infrared Phys. Technol. 77 (2016) 277–282.
[8] R. Collacott, Mechanical fault diagnosis and condition monitoring, 2012.
[9] J. de Jesus Rangel-Magdaleno, R. de Jesus Romero-Troncoso, R.A. Osornio-Rios, E. Cabal-Yepez, L.M. Contreras-Medina, Novel methodology for online half-broken-bar detection on induction motors, IEEE Trans. Instrument. Measur. 58 (5) (2009) 1690–1698.
[10] S. Guedidi, S.E. Zouzou, W. Laala, K. Yahia, M. Sahraoui, Induction motors broken rotor bars detection using MCSA and neural network: experimental research, Int. J. Syst. Assurance Eng. Manage. 4 (2) (2013) 173–181.
[11] M. Nemec, K. Drobnic, D. Nedeljkovic, R. Fiser, V. Ambrozic, Detection of broken bars in induction motor through the analysis of supply voltage modulation, IEEE Trans. Indust. Electron. 57 (8) (2010) 2879–2888.
[12] M.F. Cabanas, F. Pedrayes, C.H. Rojas, M.G. Melero, J.G. Norniella, G.A. Orcajo, D.R. Fuentes, A new portable, self-powered, and wireless instrument for the early detection of broken rotor bars in induction motors, IEEE Trans. Indust. Electron. 58 (10) (2011) 4917–4930.
[13] M.F. Cabanas, F. Pedrayes, M.G. Melero, C.H.R. Garcia, J.M. Cano, G.A. Orcajo, J.G. Norniella, Unambiguous detection of broken bars in asynchronous motors by means of a flux measurement- based procedure, IEEE Trans. Instrument. Measur. 60 (3) (2011) 891–899.
[14] A. Ceban, R. Pusca, R. Romary, Study of rotor faults in induction motors using external magnetic field analysis, IEEE Trans. Indust. Electron. 59 (5) (2012) 2082–2093.
[15] X. Ying, Performance evaluation and thermal fields analysis of induction motor with broken rotor bars located at different relative positions, IEEE Trans. Magnet. 46 (5) (2010) 1243–1250.
[16] P.A. Delgado-Arredondo, A. Garcia-Perez, D. Morinigo-Sotelo, R.A. Osornio-Rios, J.G. Avina- Cervantes, H. Rostro-Gonzalez, R.D.J. Romero-Troncoso, Comparative study of time- frequency decomposition techniques for fault detection in induction motors using vibration analysis during startup transient, Shock Vibr. (2015).
[17] B. Xu, L. Sun, H. Ren, A new criterion for the quantification of broken rotor bars in induction motors, IEEE Trans. Energy Convers. 25 (1) (2010) 100–106.
[18] R. Puche-Panadero, M. Pineda-Sanchez, M. Riera-Guasp, J. Roger-Folch, E. Hurtado-Perez, J. Perez- Cruz, Improved resolution of the MCSA method via Hilbert transform, enabling the diagnosis of rotor asymmetries at very low slip, IEEE Trans. Energy Convers. 24 (1) (2009) 52–59.
[19] G. Singh, T.C.A. Kumar, V.N.A. Naikan, Effectiveness of Current Envelope analysis to detect broken rotor bar and inter turn faults in an inverter fed induction motor drive, in: Presented at IEEE International Conference on Power and Advanced Control Engineering (ICPACE), 2015, August.
[20] S.H. Kia, H. Henao, G.A. Capolino, A high-resolution frequency estimation method for three-phase induction machine fault detection, IEEE Trans. Indust. Electron. 54 (4) (2007) 2305–2314.
[21] A. Garcia-Perez, R. de Jesus Romero-Troncoso, E. Cabal-Yepez, R.A. Osornio-Rios, The application of high-resolution spectral analysis for identifying multiple combined faults in induction motors, IEEE Trans. Indust. Electron. 58 (5) (2011) 2002–2010.
[22] H. Çalış, A. Çakır, Experimental study for sensorless broken bar detection in induction motors, Energy Convers. Manage. 49 (4) (2008) 854–862.
[23] A.K. Samanta, A. Naha, A. Routray, A.K. Deb, Fast and accurate spectral estimation for online detection of partial broken bar in induction motors, Mech. Syst. Signal Process. 98 (2018) 63–77.
[24] A. Naha, A.K. Samanta, A. Routray, A.K. Deb, Determining autocorrelation matrix size and sampling frequency for MUSIC algorithm, IEEE Signal Process. Lett. 22 (8) (2015) 1016–1020.
[25] V.F. Pires, M. Kadivonga, J.F. Martins, A.J. Pires, Motor square current signature analysis for induction motor rotor diagnosis, Measurement 46 (2) (2013) 942–948.
[26] M.H. Hayes, Statistical digital signal processing and modeling, 2009.
[27] G.K. Singh, Experimental investigations on induction machine condition monitoring and fault diagnosis using digital signal processing techniques, Elect. Power Syst. Res. 65 (3) (2003) 197–221.
[28] G.K. Singh, Induction machine drive condition monitoring and diagnostic research—a survey, Elect. Power Syst. Res. 64 (2) (2003) 145–158.
[29] A. Naha, A.K. Samanta, A. Routray, A.K. Deb, A method for detecting half-broken rotor bar in lightly loaded induction motors using current, IEEE Trans. Instrument. Measur. 65 (7) (2016) 1614–1625.
[30] H. Keskes, A. Braham, Z. Lachiri, Broken rotor bar diagnosis in induction machines through stationary wavelet packet transform and multiclass wavelet SVM, Elect. Power Syst. Res. 97 (2013) 151–157.
[31] R.J. Romero-Troncoso, A. Garcia-Perez, D. Morinigo-Sotelo, O. Duque-Perez, R.A. Osornio-Rios, M.A. Ibarra-Manzano, Rotor unbalance and broken rotor bar detection in inverter-fed induction motors at start-up and steady-state regimes by high-resolution spectral analysis, Elect. Power Syst. Res. 133 (2016) 142–148.
[32] R.A. Lizarraga-Morales, C. Rodriguez-Donate, E. Cabal-Yepez, M. Lopez-Ramirez, L.M. Ledesma- Carrillo, E.R. Ferrucho-Alvarez, Novel FPGA-based methodology for early broken rotor bar detection and classification through homogeneity estimation, IEEE Trans. Instrument. Measur. (2017).
[33] H. Çalış, A. Çakır, Rotor bar fault diagnosis in three phase induction motors by monitoring fluctuations of motor current zero crossing instants, Elect. Power Syst. Res. 77 (5) (2007) 385–392.
[34] M. Abd-el-Malek, A.K. Abdelsalam, O.E. Hassan, Induction motor broken rotor bar fault location detection through envelope analysis of start-up current using Hilbert transform, Mech. Syst. Signal Process. 93 (2017) 332–350.

[35] K.N. Gyftakis, A.J.M. Cardoso, J.A. Antonino-Daviu, Introducing the filtered park's and filtered extended park's vector approach to detect broken rotor bars in induction motors independently from the rotor slots number, Mech. Syst. Signal Process. 93 (2017) 30–50.
[36] F. Gu, T. Wang, A. Alwodai, X. Tian, Y. Shao, A.D. Ball, A new method of accurate broken rotor bar diagnosis based on modulation signal bispectrum analysis of motor current signals, Mech. Syst. Signal Process. 50 (2015) 400–413.
[37] P. Shi, Z. Chen, Y. Vagapov, Z. Zouaoui, A new diagnosis of broken rotor bar fault extent in three phase squirrel cage induction motor, Mech. Syst. Signal Process. 42 (1) (2014) 388–403.
[38] B. Xu, L. Sun, L. Xu, G. Xu, Improvement of the Hilbert method via ESPRIT for detecting rotor fault in induction motors at low slip, IEEE Trans. Energy Convers. 28 (1) (2013) 225–233.
[39] M. Pineda-Sanchez, R. Puche-Panadero, M. Riera-Guasp, J. Perez-Cruz, J. Roger-Folch, J. Pons-Llinares, V. Climente-Alarcon, J.A. Antonino-Daviu, Application of the Teager-Kaiser energy operator to the fault diagnosis of induction motors, IEEE Trans. Energy Convers. 28 (4) (2013) 1036–1044.
[40] M.A. Cruz, A.J. Marques, S. Cardoso, Rotor cage fault diagnosis in three-phase induction motors by extended Park's vector approach, Elect. Mach. Power Syst. 28 (4) (2000) 289–299.
[41] M.R. Mehrjou, N. Mariun, M.H. Marhaban, N. Misron, Rotor fault condition monitoring techniques for squirrel-cage induction machine—a review, Mech. Syst. Signal Process. 25 (8) (2011) 2827–2848.
[42] Didier Rémond, Ilyes Khelf, Lakhdar Laouar, Abdelaziz M. Bouchelaghem, Salah Saad, Adaptive fault diagnosis in rotating machines using indicators selection, Mech. Syst. Signal Process 40 (2) (2013) 452–468.
[43] L. Renaudin, F. Bonnardot, O. Musy, J.B. Doray, D. Rémond, Natural roller bearing fault detection by angular measurement of true instantaneous angular speed, Mech. Syst. Signal Process. 24 (7) (2010) 1998–2011.
[44] G. Singh, T.C.A. Kumar, V.N.A. Naikan, Efficiency monitoring as a strategy for cost effective maintenance of induction motors for minimizing carbon emission and energy consumption, Reliab. Eng. Syst. Safe. (2018).